

Inner vacuum gap formation and drifting subpulses in pulsars

Janusz A. Gil & George I. Melikidze

Institute of Astronomy, University of Zielona Góra, Lubuska 2, 65-265, Zielona Góra, Poland

Abstract. The problem of formation of the inner vacuum gap in neutron stars with $\mathbf{\Omega} \cdot \mathbf{B} < 0$ is considered. It is argued by means of the condition $T_i/T_s > 1$, where T_i is the melting temperature of surface ${}^{56}\text{Fe}$ ions and T_s is the actual temperature of the polar cap surface, that the inner vacuum gap can form, provided that the actual surface magnetic field is extremely strong ($B_s \gtrsim 10^{13}$ G) and curved ($\mathcal{R} < 10^6$ cm), irrespective of the value of dipolar component measured from the pulsar spin down rate. The calculations are carried out for pulsars with drifting subpulses and/or periodic intensity modulations, in which the existence of the quasi steady vacuum gap discharging via $\mathbf{E} \times \mathbf{B}$ drifting sparks is almost unavoidable.

1. Introduction

The subpulses in single pulses of a number of pulsars change phase systematically between adjacent pulses, forming apparent driftbands of the duration from several to few tenths of pulse periods. The subpulse intensity is also systematically modulated along driftbands, typically increasing towards the pulse centre. In some pulsars, which can be associated with the central cut of the line-of-sight trajectory, only periodic intensity modulation is observed, without a systematic change of subpulse phase. On the other hand, the clear subpulse driftbands are found in pulsars with grazing line-of-sight trajectories. These characteristics strongly suggest an interpretation of this phenomenon as a system of subpulse associated beams rotating slowly around the magnetic axis. Ruderman & Sutherland (1975; hereafter RS75) proposed a natural explanation of the origin of subpulse drift, that involved a number of isolated $\mathbf{E} \times \mathbf{B}$ drifting sparks discharging the quasi steady vacuum gap formed above the polar cap of the so-called anti-pulsar with $\mathbf{\Omega} \cdot \mathbf{B} < 0$, in which ${}^{56}\text{Fe}$ ions were strongly bound at the surface. Although the original idea of RS75 associating the rotating sub-beams with the circulating sparks is still regarded as the best qualitative model of drifting subpulse phenomenon, their vacuum gap was later demonstrated to suffer from the so-called binding energy problem (for re-

view see Abrahams & Shapiro 1991). In fact, the cohesive energies of ${}^{56}\text{Fe}$ ions used by RS75 proved to be largely overestimated and the inner vacuum gap envisioned by RS75 was impossible to form. However, it is worth to emphasize that RS75 considered the canonical surface dipolar magnetic fields with values determined from the pulsar spindown rate, although they implicitly assumed small radii of curvature $\mathcal{R} \sim 10^6$ cm, inconsistent with purely dipolar field. Recently Gil & Mitra (2001; hereafter GM01) revisited the binding energy problem and found that formation of vacuum gap is in principle possible, although it requires extremely strong non dipolar surface magnetic field $B_s = bB_d$, where the coefficient $b \gg 1$ in typical pulsar, $B_d = 6.4 \times 10^{19} (P\dot{P})^{0.5} \text{G} = 2 \times 10^{12} (P\dot{P}_{-15})^{0.5} \text{G}$ is the dipolar field at the pole, P is the pulsar period in seconds, \dot{P} is the period derivative and $\dot{P}_{-15} = \dot{P}/10^{-15}$.

In a superstrong surface magnetic field $B_s > 0.1B_q$, where $B_q = 4.414 \times 10^{13}$ G, the asymptotic approximation of Erber 1966 used by RS75 in derivation of the height of quasi steady vacuum gap is no longer valid. In fact, in such strong field the high energy $E_f = \hbar\omega$ photons produce electron-positron pairs at or near the kinematic threshold $\hbar\omega = 2mc^2/\sin\theta$, where $\sin\theta = h/\mathcal{R}$, h is the gap height, and $\mathcal{R} = \mathcal{R}_6 10^6$ cm is the radius of curvature of surface magnetic field lines (e.g. Daugherty & Harding 1983), \hbar is the Planck constant, c is the speed of light, m and e are the electron mass and charge, respectively. The vacuum gap formed under such conditions was called the Near Threshold Vacuum Gap (hereafter NTVG) by GM01. They considered two kinds of high energy seed photons dominating the e^-e^+ pair production: the Curvature Radiation (CR) photons with energy $\hbar\omega = (3/2)\hbar\gamma^3c/\mathcal{R}$ (RS75; Zhang & Qiao 1996), and resonant Inverse Compton Scattering (ICS) photons with energy $\hbar\omega = 2\gamma\hbar eB_s/mc$ (?), where γ is a typical Lorentz factor of particles within the gap. The corresponding vacuum gap is called the Curvature Radiation dominated (CR-NTVG) and the Inverse Compton Scattering dominated (ICS-NTVG), respectively. GM01 estimated the characteristic heights of both CR-NTVG and ICS-NTVG. In this paper we will further refine these estimates by including the general relativistic (GR) effects of inertial frame dragging (IFD) and

considering the heat flow conditions within the thin uppermost surface layer of the polar cap. Moreover, we will use broader range of cohesive energies of surface ^{56}Fe ions. The obtained VG models are applied to pulsars with drifting subpulses and/or periodic intensity modulations, in which the presence of $\mathbf{E} \times \mathbf{B}$ drifting spark discharges seems almost unavoidable (Deshpande & Rankin 1999; 2001; Vivekanand & Joshi 1999 and Gil & Sendyk 2000).

2. Near threshold vacuum gap formation

If the cohesive energy of ^{56}Fe ions is large enough to prevent them from thermionic (this section) or field emission (Appendix A), a vacuum gap forms right above the polar cap. Jessner et al. (2001) pointed out that the GR effect of IFD (?) should affect the RS75 type models with a vacuum gap above the polar cap. Although Jessner et al. (2001) did not investigate the problem, they implicitly suggested that the electric fields distorted by GR effects make formation of “starved” inner magnetospheric regions even more difficult than in the flat space case. However, Zhang et al. (2000) demonstrated that although the GR-IFD effect is small, it nevertheless slightly helps formation of VG above the polar caps. In other words, the GR modified potential drop within the VG is slightly lower than in the flat space case. Below we confirm this finding for NTVG conditions, with a very strong and complicated surface magnetic field.

The gap electric field \mathbf{E}_{\parallel} along \mathbf{B}_s results from a deviation of the local charge density $\rho \approx 0$ from the corotational charge density $\rho_c = (\zeta/\alpha)\rho_{GJ}$, where $\rho_{GJ} = -\mathbf{\Omega} \cdot \mathbf{B}_s/(2\pi c)$ is the flat space-time Goldreich-Julian (1969) charge density, $\Omega = 2\pi/P$, $\zeta = 1 - \kappa_g$, $\kappa_g \sim (r_g/R)(I/MR^2)$, $\alpha = (1 - r_g/R)^{1/2}$ is the redshift factor, r_g is the gravitational radius, M is the neutron star mass and I is the neutron star moment of inertia. The potential V and electric fields E_{\parallel} within a gap are determined by GR-analog (Muslimov & Tsygan 1992) of the one dimensional Poisson’s equation $(1/\alpha)d^2V/dz^2 = -4\pi(\rho - \rho_c) = 2\Omega B_s \zeta / (c\alpha)$, with a boundary condition $E_{\parallel}(z = h) = 0$, where h is the height of infinitesimal gap. The solution of Poisson’s equation gives

$$E_{\parallel}(z) = \zeta(2\Omega \frac{B_s}{c})(h - z) \quad (1)$$

and

$$\Delta V = \zeta \frac{\Omega B_s}{c} h^2. \quad (2)$$

In further calculations we will adopt a typical value of the correction factor $\zeta \sim 0.85$ (corresponding to $M = 1M_{\odot}$, $R = 10^6$ cm and $I = 10^{45}$ g cm²), although its value can be as low as 0.73 (Zhang et al. 2000). Thus, the potential drop within the actual gap can be 15 to 27 percent lower than in the conventional RS75 model.

The polar cap surface of the anti-pulsar ($\mathbf{\Omega} \cdot \mathbf{B} < 0$) is heated by a back-flow of relativistic electrons (accelerated in the parallel electric field E_{\parallel}) to the temperature $T_s =$

$k^{1/4}(e\Delta V \dot{N} / \sigma \pi r_p^2)^{1/4}$, where ΔV is described by equation (2), $\dot{N} = \pi r_p^2 B_s / eP$ is the Goldreich-Julian kinematic flux and the heat flow coefficient $0.2 \lesssim k < 1$ is described in the Appendix B. The thermal condition for the vacuum gap formation can be written in the form $T_i/T_s > 1$, where T_s is the actual surface temperature described above, and $T_i = \Delta \varepsilon_c / 30k$ is the iron critical (melting) temperature above which ^{56}Fe ions are not bound on the surface (?), where $\Delta \varepsilon_c$ is the cohesive energy of condensed ^{56}Fe matter in the neutron star surface and $k = 1.38 \times 10^{-23} JK^{-1}$ is the Boltzman constant. The properties of condensed matter in very strong magnetic fields characteristic for the neutron star surface have been investigated by many authors using different examination methods (for review see Usov & Melrose 1995). There exists a lot of discrepancy in determination of the cohesive energy $\Delta \varepsilon_c$ and in this paper we refer to the two most useful papers, representing the limiting extreme cases. Abrahams & Shapiro (1991; AS91 henceforth) estimated $\Delta \varepsilon_c = 0.91$ keV, 2.9 keV and 4.9 keV for $B_s = 10^{12}$ G, 5×10^{13} G and 10^{13} G, respectively. These values were approximated by Usov & Melrose 1995 in the form $\Delta \varepsilon_c \simeq (0.9\text{keV})(B_s/10^{12} \text{ G})^{0.73}$, which leads to melting temperatures

$$T_i = (3.5 \times 10^5 \text{K})(B_s/10^{12} \text{G})^{0.73} = (6 \times 10^5) b^{0.73} (P \dot{P}_{-15})^{0.36} \text{ K}. \quad (3)$$

On the other hand, Jones (1986; J86 henceforth) obtained much lower cohesive energies $\Delta \varepsilon_c = 0.29$ keV, 0.60 keV and 0.92 keV for $B_s = 2 \times 10^{12}$ G, 5×10^{12} G and 10^{13} G, respectively. This can be approximated by $\Delta \varepsilon_c \simeq (0.18 \text{ keV})(B_s/10^{12} \text{G})^{0.7}$ and converted to melting temperatures

$$T_i = (0.7 \times 10^5 \text{K})(B_s/10^{12} \text{G})^{0.7} = (1.2 \times 10^5) b^{0.7} (P \cdot \dot{P}_{-15})^{0.36}. \quad (4)$$

Below we consider the condition $T_i/T_s > 1$, using both expressions for melting temperatures described by equations (3) and (4), for CR- and ICS-dominated NTVG models, separately.

2.1. CR-NTVG

In this case the gap height $h = h_{CR}$ is determined by the condition that $h = l_{ph}$, where $l_{ph} \approx \sin \theta \mathcal{R} = (B_{\perp}/B_s)\mathcal{R}$ is the mean free path for pair production by photon propagating at an angle θ to the local surface magnetic field (RS75). The CR-NTVG model is described by the following parameters: the height of quasi steady gap

$$h_{CR} = (3 \times 10^3) \zeta^{-3/7} \mathcal{R}_6^{2/7} b^{-3/7} P^{3/14} \dot{P}_{-15}^{-3/14} \text{ cm}, \quad (5)$$

(notice typographical errors in eq. [6] of GM01, which are corrected here), the gap potential drop

$$\Delta V = (1.2 \times 10^{12}) \zeta^{1/7} \mathcal{R}_6^{4/7} b^{-1/7} P^{-1/14} \dot{P}_{-15}^{1/14} \text{ V}, \quad (6)$$

and the surface temperature

$$T_s = (3.4 \times 10^6) \zeta^{1/28} k^{1/4} \mathcal{R}_6^{1/7} b^{2/7} P^{-1/7} \dot{P}_{-15}^{1/7} \text{ K.} \quad (7)$$

The thermal condition $T_i/T_s > 1$ for the formation of CR-NTVG leads to a family of critical lines on the $P - \dot{P}$ diagram (see Fig. 1 in GM01)

$$\dot{P}_{-15} \geq \mathcal{A}^2 \zeta^{0.16} k^{1.14} \mathcal{R}_6^{0.64} b^{-2} P^{-2.3}, \quad (8)$$

where $\mathcal{A} = (2.7 \times 10^3)^{1/2} = 52$ for AS91 case (eq. [3]) and $\mathcal{A} = (3.96 \times 10^6)^{1/2} = 1990$ for J86 case (eq. [4]). Alternatively, one can find a minimum required surface magnetic field $B_s = bB_d$ expressed by the coefficient b in the form

$$b_{min}^{CR} = \mathcal{A} \zeta^{0.08} k^{0.57} \mathcal{R}_6^{0.32} P^{-1.15} \dot{P}_{-15}^{-0.5}. \quad (9)$$

2.2. ICS-NTVG

In this case the gap height $h = h_{ICS}$ is determined by the condition $h = l_{ph} \sim l_e$, where l_e is the mean free path of the electron to emit a photon with energy $\hbar\omega = 2\gamma\hbar eB_s/mc$ (GM01, Zhang et al. 2000). The ICS-NTVG model is described by the following parameters: the height of quasi steady gap

$$h_{ICS} = (5 \times 10^3) \zeta^{0.14} k^{-0.07} \mathcal{R}_6^{0.57} b^{-1} P^{-0.36} \dot{P}_{-15}^{-0.5} \text{ cm,} \quad (10)$$

the gap potential drop

$$\Delta V = (5.2 \times 10^{12}) \zeta^{0.72} k^{-0.14} \mathcal{R}_6^{1.14} b^{-1} P^{-1.22} \dot{P}_{-15}^{-0.5} \text{ V,} \quad (11)$$

and the surface temperature

$$T_s = (4 \times 10^6) \zeta^{0.18} k^{0.25} \mathcal{R}_6^{0.28} P^{-0.43} \text{ K.} \quad (12)$$

The thermal condition $T_i/T_s > 1$ for the formation of ICS-NTVG leads to a family of critical lines on the $P - \dot{P}$ diagram (see Fig. 1 in GM01)

$$\dot{P}_{-15} \geq \mathcal{B}^2 \zeta^{0.5} k^{0.7} \mathcal{R}_6^{0.8} b^{-2} P^{-2.2}, \quad (13)$$

where $\mathcal{B} = (2 \times 10^2)^{1/2} = 14$ for AS91 case (eq. [3]) and $\mathcal{B} = (1.69 \times 10^4)^{1/2} = 130$ for J86 case (eq. [4]). Alternatively, one can find a minimum required surface magnetic field $B_s = bB_d$ expressed by the coefficient b in the form

$$b_{min}^{ICS} = \mathcal{B} \zeta^{0.25} k^{0.34} \mathcal{R}_6^{0.39} P^{-1.1} \dot{P}_{-15}^{-0.5}. \quad (14)$$

2.3. NTVG development in pulsars with drifting subpulses

GM01 examined the $P - \dot{P}$ diagram (their Fig. 1) with 538 pulsars from the Pulsar Catalog (Taylor et al. 1993) with respect to the possibility of VG formation by means of the condition T_i/T_s , with T_i determined according to AS91 (eq. [3]). They concluded that formation of VG is in principle possible, although it requires very strong and

curved surface magnetic field $B_s = b \cdot B_d \gtrsim 10^{13}$ G, irrespective of the value of B_d . Here we reexamine this problem by means of equations (9) and (14), with melting temperatures corresponding to both the AS91 case ($\mathcal{A} = 52$ and $\mathcal{B} = 14$) and J86 case ($\mathcal{A} = 1990$ and $\mathcal{B} = 130$), for CR and ICS seed photons, respectively. Therefore, we cover practically almost the whole range of melting temperatures between the two limiting cases, which differ by a factor of five between each other. We adopt the GR-IFD correction factor $\zeta = 0.85$ (?), the normalized radius of curvature of surface magnetic field lines $0.01 \leq \mathcal{R}_6 \leq 1.0$ (GM01 and references therein) and the heat flow coefficient $0.2 \leq k \leq 1.0$ (Appendix B).

The results of calculations of NTVG models for 42 pulsars with drifting subpulses and/or periodic intensity modulations (after Rankin 1986) are presented in Fig. 1. We calculated the ratio $B_s/B_q = 0.0453 b(P\dot{P}_{-15})^{0.5}$, where $B_q = 4.414 \times 10^{13}$ G and the coefficient b is determined by equation 9 and equation 14 for CR and ICS seed photons, respectively. Noting that the functional dependence on P and \dot{P}_{-15} in both equations is almost identical, we sorted the pulsar names (shown on the horizontal axes) according to the increasing value of the ratio B_s/B_q (shown on the vertical axes). Calculations were carried out for $B_s/B_q \geq 0.1$, since below this value the NT conditions are no longer valid. On the other hand, the values of B_s/B_q are limited from above by the photon splitting threshold, which is roughly about 10^{14} G (see also astro-ph/0102097, ?). Therefore, the physically plausible NTVG models lie within the grey areas, which correspond to surface magnetic fields $4.4 \times 10^{12} \text{ G} \leq B_s \leq 10^{14} \text{ G}$. The left hand side of Fig. 1 corresponds to AS91 case ($\mathcal{A} = 52$ and $\mathcal{B} = 14$ in eqs. [9] and [14], respectively) and the right hand side of Fig. 1 corresponds to J86 case ($\mathcal{A} = 1930$ and $\mathcal{B} = 130$ in eqs. [9] and [14], respectively). Four panels in each side of the figure correspond to different values of the radius of curvature $\mathcal{R}_6 = 1.0, 0.1, 0.05$ and 0.01 from top to bottom, respectively (indicated in left upper corner of each panel). Two sets of curved lines in each panel correspond to the CR (thin upper lines) and ICS (thick lower lines) seed photons, respectively. Three different lines within each set correspond to different values of the heat flow coefficient $k = 1.0$ (dotted), $k = 0.6$ (dashed) and $k = 0.2$ (long dashed).

A visual inspection of the model curves within grey areas in Fig. 1 shows that in AS91 case the ICS-NTVG is favored for larger radii of curvature $\mathcal{R}_6 > 0.05$, while the CR-NTVG requires lower values of $\mathcal{R}_6 < 0.1$. In J86 case, only the ICS-NTVG corresponding to $\mathcal{R}_6 < 0.1$ can develop. If the actual cohesive energies correspond to some intermediate case between the AS91 and J86 cases, they will also be associated with the ICS-NTVG. Therefore, we can generally conclude that the ICS-NTVG model is apparently favored in pulsars with drifting subpulses. The CR-NTVG is also possible although it requires an

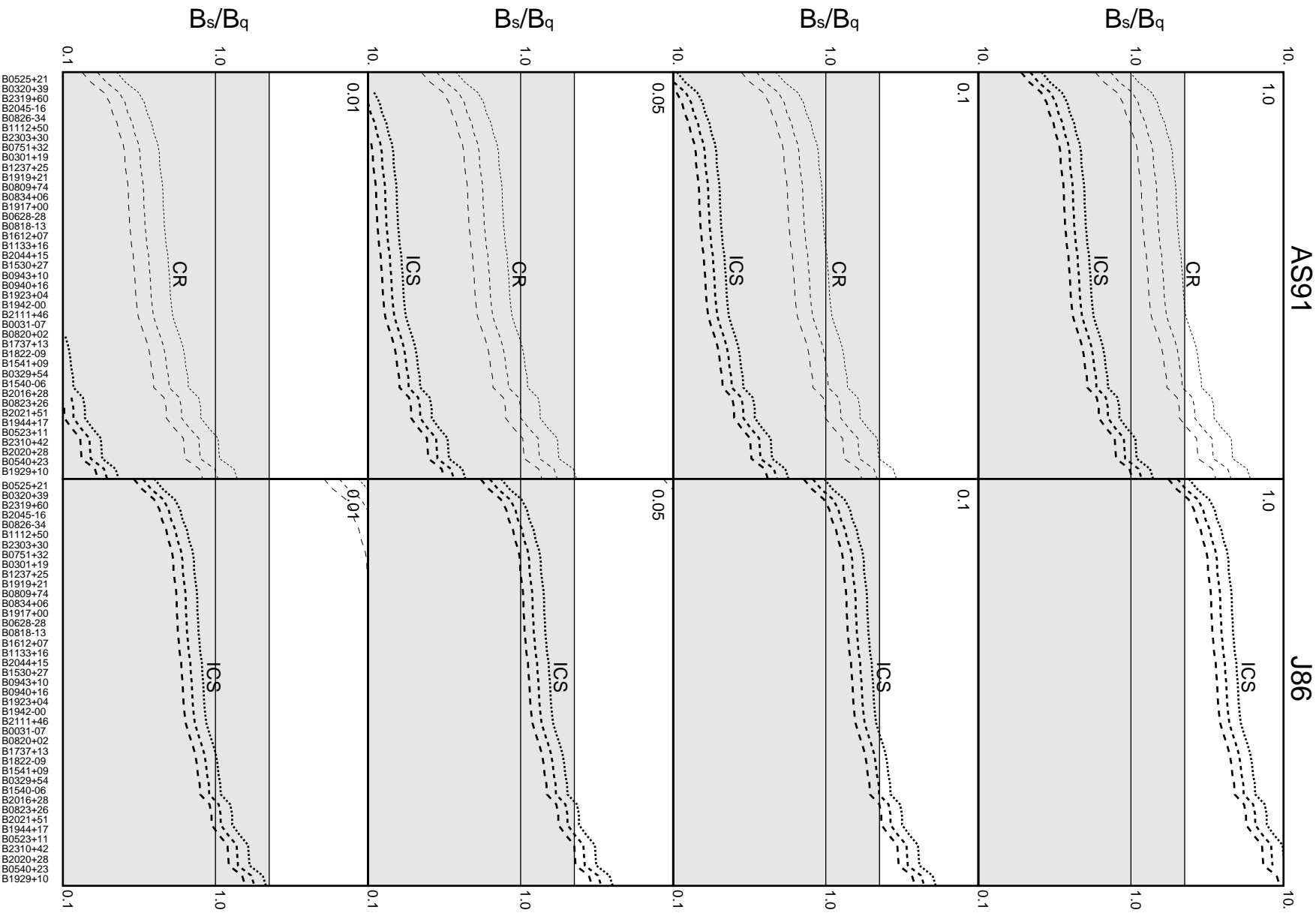


Fig. 1. Models of NTVG for 42 pulsar with drifting subpulses and/or periodic intensity modulations (see text for explanations).

extremely strong ($B_s/B_q \sim 1$) and/or extremely curved ($\mathcal{R}_6 \sim 0.01$) surface magnetic field at the polar cap.

3. Conclusions

There is a growing evidence that the radio emission of pulsars with systematically drifting subpulses (grazing cuts of the line-of-sight) or periodic intensity modulations (central cuts of the line-of-sight) is based on the inner vacuum gap developed just above the polar cap (?). To overcome the binding energy problem (?) put forward an attractive but exotic conjecture that pulsars showing the drifting subpulses represent bare polar cap strange stars (BPCSS) rather than neutron stars. However, as demonstrated in this paper, invoking the BPCSS conjecture is not necessary to explain drifting subpulse phenomenon. The quasi steady vacuum gap, with either curvature radiation or inverse Compton scattering seed photons, can easily form in pulsars with $\boldsymbol{\Omega} \cdot \mathbf{B} < 0$, provided that the actual surface magnetic field at the polar cap is extremely strong $B_s \sim 10^{13}$ G and curved $\mathcal{R} < 10^6$ cm, irrespective of the value of dipolar component measured from the pulsar spindown rate.

The pulsars with drifting subpulses and/or periodic intensity modulation do not seem to occupy any particular region of the $P - \dot{P}$ diagram (see Fig. 1 in GM01). Rather, they are spread uniformly all over the $P - \dot{P}$ space, at least for typical pulsars. Therefore, it seems tempting to propose that radio emission of all pulsars is driven by vacuum gap activities. An attractive property of such proposition is that the nonstationary sparking discharges induce the two-stream instabilities that develop at relatively low altitudes (?), where the pulsars radio emission is expected to originate (?). It is generally believed that the high frequency plasma waves generated by the two-stream instabilities can be converted into coherent electromagnetic radiation at pulsar radio wavelengths (e.g. Melikidze et al. 2000). In such a scenario, all radio pulsars would require a strong, non-dipolar surface magnetic field at their polar caps (e.g. Gil et al. 2002 a, b).

Acknowledgements. We gratefully acknowledge the support by the Heraeus foundation. We are grateful to Prof. V. Usov and dr B. Zhang for helpful discussions. We also thank E. Gil, U. Maciejewska, and M. Sendyk for technical help.

Appendix A: Field emission

The vacuum gap can form in pulsars with $\boldsymbol{\Omega} \cdot \mathbf{B} < 0$ if the actual surface temperature T_s is not high enough to liberate ^{56}Fe ions from the polar cap surface by means of thermal emission. Now we will examine the field (cold cathode) emission, which is possibly important when thermionic emission is negligible (e.g. Zhang & Harding 2000). The maximum electric field (along \mathbf{B}_s) at the NS surface $E_{\parallel}(max) = \zeta(4\pi/cP)B_s h_{ICS} = (1.25 \times 10^9)\zeta^{0.86}b^{-1}\mathcal{R}_6^{0.57}P^{0.14}$ V/cm,

or taking into account that $\zeta = 0.85$ and $b \gtrsim 2(P \cdot \dot{P}_{-15})^{-0.5}$, $E_{\parallel}(max) \leq (5 \times 10^8)\mathcal{R}_6^{0.57}P^{0.64}\dot{P}_{-15}^{0.5}$ V/cm. The critical electric field needed to pull ^{56}Fe iron ions from the NS surface is $E_{\parallel}(crit) = (8 \times 10^{12})(\Delta\epsilon/26 \text{ keV})^{3/2}$ V/cm (?), where the cohesive (binding) energy of iron ions in strong surface magnetic field $B_s \sim 10^{13}$ G is $\Delta\epsilon = 4.85$ keV (Abrahams & Shapiro 1991). Thus, $E_{\parallel}(crit) = 6.4 \times 10^{11}$ V/cm $\gg E_{\parallel} \sim 10^9$ V/cm and no field emission occurs. It is possible that the cohesive energy is largely overestimated and $\Delta\epsilon_c$ can be much smaller than about 4 keV even at $B_s > 10^{13}$ G. We can thus ask about the minimum value of $\Delta\epsilon_c$ at which the field emission is still negligible. By direct comparison of $E_{\parallel}(max)$ and $E_{\parallel}(crit)$ we obtain $\Delta\epsilon_c > 40x^{0.67}$ eV, where $x = \mathcal{R}_6^{0.57}P^{0.64}\dot{P}_{-15}^{0.5}$ is of the order of unity. Therefore, contrary to the conclusion of Jessner et al. (2001), no field emission is expected under any circumstances.

Appendix B: Heat flow conditions at the polar cap surface

Let us consider the heat flow conditions within the uppermost surface layer of the pulsar polar cap above which NTVG can develop. The basic heat flow equation is (e.g. Eichler & Cheng 1989)

$$C \frac{\partial T}{\partial t} = \frac{\partial}{\partial x} \left(\kappa_{\parallel} \frac{\partial T}{\partial x} \right), \quad (\text{B1})$$

where C is the heat capacity (per unit volume) and $\kappa_{\parallel} \gg \kappa_{\perp} \sim 0$ is the thermal conductivity along (\parallel) surface magnetic field lines (which are assumed to be perpendicular (\perp) to the polar cap surface). The heating of the surface layer of thickness Δx is due to sparking avalanche with a characteristic development time scale Δt . We can write approximately $\partial T/\partial t \approx T/\Delta t$, $\partial T/\partial x \approx T/\Delta x$, $\partial/\partial x(\partial T/\partial x) \approx T/\Delta x^2$ and thus $C/\Delta t \approx \kappa_{\parallel}/\Delta x^2$. Therefore, the crust thickness Δx heated during Δt is approximately $\Delta x \approx (\kappa_{\parallel}\Delta t/C)^{1/2}$ (within an uncertainty factor δx of 2 or so), where the time scale corresponds to the spark development time $\Delta t \approx 10\mu\text{s}$ (RS75). The energy balance equation is $Q_{heat} = Q_{rad} + Q_{cond}$, where $Q_{heat} = en_{GJ}\Delta V_{max}$ (e.g. RS75), $Q_{rad} = \sigma T_s^4$ (T_s is the actual surface temperature and $\sigma = 5.67 \times 10^{-5}$ erg cm $^{-2}$ K $^{-4}$ s $^{-1}$), and $Q_{cond} = -\kappa_{\parallel}\partial T/\partial x \approx -\kappa_{\parallel}T_s/\Delta x$. We can now define the heat flow coefficient $k = Q_{rad}/Q_{heat} < 1$, which describes deviations from the black-body conditions on the surface of the sparking polar cap. In other words, the value of k describes the amount of heat conducted beneath the polar cap which cannot be transferred back to the surface from the penetration depth Δx during the time-scale Δt . The coefficient k can be written in the form

$$k = \frac{1}{1 + \kappa_{\parallel}/(\sigma T_s^3 \Delta x)} = \frac{1}{1 + (\kappa_{\parallel}C)^{1/2}/(\sigma T_s^3 \Delta t^{1/2})}, \quad (\text{B2})$$

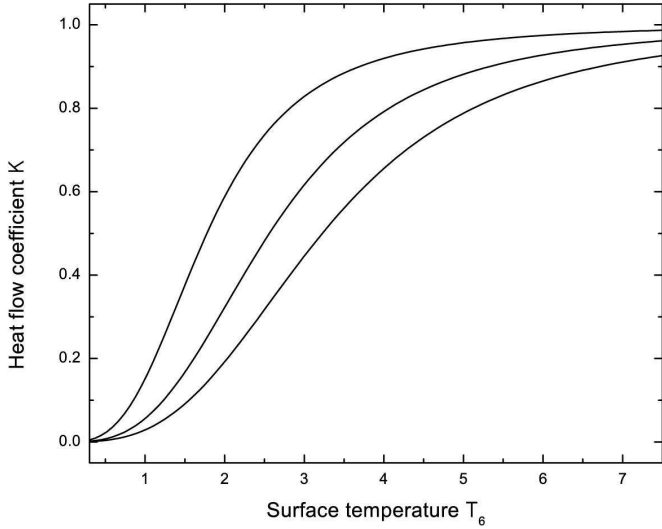


Fig. B1. Heat flow coefficient k versus surface temperature T_6 (see text for explanations).

whose value can be estimated once the parameters C , κ_{\parallel} and T_s as well as Δx or Δt are known.

The matter density at the neutron star surface composed mainly of ${}^{56}_{26}\text{Fe}$ ions (e.g. Usov & Melrose 1995) is $\rho(B_s) \simeq 4 \times 10^3 (B_s/10^{12} \text{ G})^{6/5} \text{ g cm}^{-3}$ (Flowers et al. 1977). Thus for $B_s \sim (1 \div 3) \times 10^{13} \text{ G}$ we have $\rho \sim (0.6 \div 2.4) \times 10^5 \text{ g cm}^{-3}$. The thermal energy density of ${}^{56}_{26}\text{Fe}$ is $U_{Fe} \simeq 2.2 \times 10^{19} \rho_5 T_8 \text{ erg cm}^{-3}$ (Eichler & Cheng 1989), where $\rho_5 = \rho/(10^5 \text{ g cm}^{-3})$ and $T_8 = T_s/(10^8 \text{ K})$. Thus, the heat capacity $C = dU_{Fe}/dT_8 = 10^{-8} dE_{Fe}/dT_8 = (1 \div 5) \times 10^{11} \rho_5 \text{ erg cm}^{-3} \text{ K}^{-1}$. For $\rho_5 \approx 1$ we have $C \approx 2 \times 10^{11} \text{ erg cm}^{-3} \text{ K}^{-1}$. The longitudinal thermal conductivity can be estimated as $\kappa_{\parallel} \approx (2 \div 4) \times 10^{13} \text{ erg s}^{-1} \text{ cm}^{-1} \text{ K}^{-1}$ (see Fig. 5 in Potekhin 1999). Thus $\kappa_{\parallel}/C \approx 1.5 \times 10^2 \text{ cm}^2$ and the penetration depth $\Delta x \approx 10 \Delta t^{1/2} s^{-1/2} \text{ cm}$. Since $\Delta t \sim 10 \mu = 10^{-5} \text{ s}$ (spark characteristic time scale) then $\Delta x \approx 0.03 \text{ cm}$. More generally, the penetration depth can be written as

$$\Delta x = 0.03 \delta x \left(\frac{\kappa_{13}}{C_{11}} \right)^{1/2}, \quad (\text{B3})$$

where $\kappa_{13} = \kappa_{\parallel}/10^{13} \approx 2 \div 4$ and $C_{11} = C/10^{11} \approx 1 \div 5$ and the uncertainty factor $\delta x \approx 0.5 \div 2$. Now the heat flow coefficient can be written as

$$k = \frac{1}{1 + 5.6 \Delta / T_6^3}, \quad (\text{B4})$$

where $T_6 = T_s/10^6$ and $\Delta = (\kappa_{13} C_{11})^{1/2} / \delta x \approx 0.7 \div 6.3$. Figure 2 shows variations of the heat flow coefficient k versus the surface temperature T_6 (in 10^6 K) for three values of $\Delta = 1$ (upper curve), $\Delta = 3$ (middle curve) and $\Delta = 6$ (lower curve). As one can see, for realistic surface temperatures of few times 10^6 K , the values of the heat flow coefficient k are in the range $0.2 \div 0.9$. Gil et al. 2002a found

from independent considerations that in PSR B0943+10 the heat flow coefficient $k < 0.8$, in consistency with the results obtained in this paper.

References

- Abrahams, A.M., Shapiro, S.L. 1991, ApJ, 374, 652
 Asseo, E., Melikidze, G. 1998, MNRAS 301, 59
 Cheng, A. F., & Ruderman, M. A. 1977, ApJ, 212, 800
 Cheng, A. F., & Ruderman, M. A. 1980, ApJ, 235, 576
 Cordes, J. M. 1978, ApJ, 222, 1006
 Barrington, M.G., Harding, A.K. 1998, ApJ, 507, L55
 Barrington, M.G., Harding, A.K. 2001, ApJ, 547, 926
 Daugherty, J., Harding, A.K. 1983, ApJ, 273, 761
 Deshpande, A.A., & Rankin, J.M. 1999, ApJ, 524, 1008
 Deshpande, A.A., & Rankin, J.M. 2001, MNRAS, 322, 438
 Eichler, D., Cheng, A.F. 1989, ApJ, 336, 360
 Erber, T. 1966, Rev. Mod. Phys., 38, 626
 Flowers, E.G., Ruderman, M.A., Lee J-F. et al. 1977, ApJ, 215, 291
 Gil, J., & Sendyk, M. 2000, ApJ, 541, 351
 Gil, J., & Mitra, D. 2001, ApJ, 550, 383 (GM01)
 Gil, J., Melikidze, G.I., & Mitra, D. 2002a, A&A Letters, in press
 Gil, J., Melikidze, G.I., & Mitra, D. 2002b, A&A, in press
 Harding, A.K., Muslimov, A.G. 1998, ApJ, 508, 328
 Jessner, A., Lesch, H., & Kunzl., T. 2001, ApJ, 547, 959
 Jones, P.B. 1986, MNRAS, 218, 477 (J86)
 Kijak, J., & Gil, J. 1997, MNRAS, 288, 631
 Kijak, J., & Gil, J. 1998, MNRAS, 299, 855
 Melikidze, G.I, Gil, J., & Pataraya, A.D. 2000, ApJ, 544, 1081
 Muslimov, A.G., Tsygan, A.I., 1992, MNRAS, 255, 61
 Muslimov, A.G., Harding, A. 1997, ApJ, 485, 735
 Potekhin, A.Y. 1999, A&A, 351, 787
 Rankin, J.M. 1986, ApJ, 301, 901
 Ruderman, M.A., & Sutherland, P.G. 1975, ApJ 196, 51 (RS75)
 Taylor, J. H., Manchester, R. N., & Lyne, A. G. 1993, ApJs, 88, 529
 Usov, V.V. 1987, ApJ, 481, L107
 Usov, V.V., & Melrose, D.B. 1995, Australian J. Phys. 48, 571
 Usov, V.V., & Melrose, D.B. 1996, ApJ, 463, 306
 Usov, V. 2001, ApJ, 559, L135
 Vivekanand, M., Joshi, B.C. 1999, ApJ, 515, 398
 Xu, R.X., Qiao, G.J., & Zhang, B. 1999, ApJ, 522, L109
 Xu, R.X., Zhang, B. & Qiao, G.J. 2001, Astropart.Phys., 15(1), 101
 Zhang, B., Qiao, G.J. 1996, A&A, 310, 135
 Zhang, B., Qiao, G.J., Lin, W.D., et al. 1997, ApJ, 478, 313
 Zhang, B., & Harding, A.K. 2000, ApJ, 535, L51
 Zhang B., Harding, A., & Muslimov, A.G. 2000, ApJ, 531, L135
 Zhang, B. 2001, ApJ, 562, L59